

This work was written as part of one of the author's official duties as an Employee of the United States Government and is therefore a work of the United States Government. In accordance with 17 U.S.C. 105, no copyright protection is available for such works under U.S. Law.

Public Domain Mark 1.0

<https://creativecommons.org/publicdomain/mark/1.0/>

Access to this work was provided by the University of Maryland, Baltimore County (UMBC) ScholarWorks@UMBC digital repository on the Maryland Shared Open Access (MD-SOAR) platform.

**Please provide feedback**

Please support the ScholarWorks@UMBC repository by emailing [scholarworks-group@umbc.edu](mailto:scholarworks-group@umbc.edu) and telling us what having access to this work means to you and why it's important to you. Thank you.

## An improved algorithm for retrieving surface downwelling longwave radiation from satellite measurements

Yaping Zhou,<sup>1</sup> David P. Kratz,<sup>2</sup> Anne C. Wilber,<sup>3</sup> Shashi K. Gupta,<sup>3</sup> and Robert D. Cess<sup>4</sup>

Received 17 October 2006; revised 13 April 2007; accepted 17 May 2007; published 3 August 2007.

[1] Zhou and Cess (2001) developed an algorithm for retrieving surface downwelling longwave radiation (SDLW) based upon detailed studies using radiative transfer model calculations and surface radiometric measurements. The algorithm links clear sky SDLW with surface upwelling longwave (LW) flux and column precipitable water vapor. For cloudy sky cases, the cloud liquid water path is used as an additional parameter to account for the effects of clouds. Despite the simplicity of the algorithm, it performs very well for most geographical regions except for those regions where the atmospheric conditions near the surface tend to be extremely cold and dry. Systematic errors are also found for scenes that are covered with ice clouds. An improved version of the algorithm prevents the large errors in the SDLW at low water vapor amounts by taking into account that, under such conditions, the SDLW and water vapor amount are nearly linear in their relationship. The new algorithm also utilizes cloud fraction and cloud liquid and ice water paths available from the Cloud and the Earth's Radiant Energy System (CERES) single-scanner footprint (SSF) product to separately compute the clear and cloudy portions of the fluxes. The new algorithm has been validated against surface measurements at 29 stations around the globe for Terra and Aqua satellites. The results show significant improvement over the original version. Preliminary tests also suggest that the new algorithm works quite well for high elevation locations such as Tibet site where current satellite products exhibit large biases. The revised Zhou-Cess algorithm is also slightly better or comparable to more sophisticated algorithms currently implemented in the CERES processing and will be incorporated as one of the CERES empirical surface radiation algorithms.

**Citation:** Zhou, Y., D. P. Kratz, A. C. Wilber, S. K. Gupta, and R. D. Cess (2007), An improved algorithm for retrieving surface downwelling longwave radiation from satellite measurements, *J. Geophys. Res.*, 112, D15102, doi:10.1029/2006JD008159.

### 1. Introduction

[2] The surface longwave (LW) fluxes are major components of the energy budget in the Earth's climate system. Developing a global, long-term surface radiation database is essential in monitoring the Earth's climate, radiation, and hydrological systems. Since direct measurements of surface radiation fluxes are expensive and will always be limited, it is desirable that satellites provide global measurements of the surface radiation fluxes. However, since the surface downwelling longwave flux and top of atmosphere outgoing longwave flux are largely decoupled, especially in cloudy skies [Ramanathan, 1986; Stephens and Webster, 1984], satellite retrievals of surface downwelling longwave

fluxes have to rely heavily on retrieved meteorological profiles, cloud parameters, and radiative transfer models to compute the surface downwelling flux, such as those adopted by the International Satellite Cloud Climatology Project (ISCCP) [Zhang *et al.*, 2004] and Global Energy and Water Cycle Experiment — Surface Radiation Budget (GEWEX-SRB) [Cox *et al.*, 2006].

[3] Using detailed studies based upon radiative transfer model calculations and surface radiometric measurements, Zhou and Cess [2001] formulated algorithm development strategies for retrieving surface downwelling longwave radiation (SDLW). Their studies demonstrated that clear sky SDLW could be largely determined by surface upwelling longwave flux and column precipitable water vapor. For cloudy sky cases, they used cloud liquid water path as an additional parameter to account for the effects of clouds instead of using cloud base height which is theoretically a more direct factor in determining the SDLW. An illustrative algorithm was derived and tested using observational data from the Atmospheric Radiation Measurements (ARM) Program [Stokes and Schwartz, 1994] measurements at the U.S. Southern Great Plain (SGP) and Tropical Western Pacific (TWP) sites.

<sup>1</sup>Goddard Earth Sciences & Technology Center, University of Maryland Baltimore County, Catonsville, Maryland, USA.

<sup>2</sup>Climate Science Branch, NASA Langley Research Center, Hampton, Virginia, USA.

<sup>3</sup>Analytical Services & Materials, Inc., Hampton, Virginia, USA.

<sup>4</sup>Marine Sciences Research Center, S.U.N.Y. at Stony Brook, Stony Brook, New York, USA.

[4] Since the algorithm was derived and tested for mid-latitude and tropical conditions, there was concern that the algorithm might not perform well for extremely cold and dry conditions. Indeed, once data had become available from the ARM North Slope of Alaska (NSA) [Stamnes *et al.*, 1999], large biases were found when the algorithm was applied to surface measurements from that location. Sensitivity studies demonstrated that the algorithm significantly underestimates SDLW when atmospheric water vapor was low.

[5] Meanwhile, the Cloud and the Earth's Radiant Energy System [CERES; Wielicki *et al.*, 1996] Surface Radiation Budget (SRB) team started to test the algorithm for possible global application. The CERES program is designed to provide crucial cloud and radiation measurements for studying cloud-radiation interaction. CERES instruments were launched aboard the Tropical Rainfall Measuring Mission (TRMM) in November 1997 and on the Earth Observation System (EOS) Terra satellite in December 1999 and Aqua satellite in May 2002. The space-borne CERES radiometers provide broadband total, shortwave (SW), and infrared window measurements at the top of atmosphere (TOA). Differencing the SW from the total measurements allows for a derivation of the longwave (LW) value. Deriving reliable estimates of SRB parameters is another important objective of the CERES project whose goal is to provide a complete picture of the energy budget of the Earth's atmosphere system. Since the SRB cannot be directly measured by satellite-borne instruments, the surface fluxes are derived with several different methods using combinations of radiation models, data assimilation products, and satellite measurements. The Surface and Atmospheric Radiation Budget [SARB; Charlock *et al.*, 1997] component of CERES represents one such method where shortwave and longwave fluxes at the surface, at three levels in the atmosphere, and at the TOA are computed with a radiative transfer model. In addition to SARB, surface fluxes are being derived within CERES using two SW and two LW models, which are based on TOA-to-surface transfer algorithms or fast radiation parameterizations. These models are by Li *et al.* [1993] (SW model A, clear sky only); Darnell *et al.* [1992] (SW model B); Inamdar and Ramanathan [1997] (LW model A, clear sky only); and Gupta *et al.* [1992] (LW model B). These models were incorporated into CERES products to provide independent sources of surface fluxes to compare with SARB results [Gupta *et al.*, 2004]. The model designed by Inamdar and Ramanathan [1997] derives clear sky downwelling longwave flux through exploring the relationships between normalized surface longwave flux and green house parameter in the window and non-window spectral regions. The model by Gupta *et al.* [1992] computes surface downwelling longwave using a parameterized formula that requires an estimation of effective emitting temperature of the atmosphere, total column water amount for clear sky and a cloud forcing factor that utilizes cloud base temperature and water vapor amount below the cloud base. The Zhou-Cess algorithm represents a new methodology for deriving SDLW globally for both clear sky and cloudy sky using surface upwelling longwave flux, column water vapor, and cloud water path that are readily available from the satellite measurements. A vigorous test was performed on instanta-

neous flux derived by Zhou-Cess algorithm as part of single-scanner footprints (SSF) products on board Terra and Aqua satellites against matched ground measurements from surface radiation measurement sites around the globe. Despite the simplicity of their algorithm, it performed very well for most of the geographical regions. Large biases, however, were found for certain regions, most notably the Polar Regions, where the atmosphere is extremely cold and dry. In addition, systematic errors were found for regions covered with ice clouds.

[6] The modifications to the algorithm discussed in the present work are aimed at addressing the low water vapor (including situations associated with high elevations such as Tibet plateau) and ice cloud situations with the goal of making the algorithm applicable for global implementation in the CERES processing. In section 2, a brief description of the original algorithm will be given followed by bias analysis of the algorithm when applied to ARM NSA data. In section 3, the algorithm is revised using collocated CERES cloud parameters and surface radiation measurements. The new algorithm is validated for CERES Terra and Aqua satellites with surface measurements from global network. In addition, a preliminary test and discussion on the application of the new algorithm on Tibet site are provided. A summary and discussions of this work are given in section 4.

## 2. Low Water Vapor Bias

### 2.1. Original Algorithm

[7] The Zhou-Cess algorithm took the form:

$$\text{SDLW} = a + b \cdot \text{SULW} + c \cdot \ln(\text{PWV}) + d \cdot [\ln(\text{PWV})]^2 + e \cdot \ln(1 + f \cdot \text{LWP}) \quad (1)$$

where SULW is the surface upwelling longwave flux computed from the 2-m air temperature using Stefan-Boltzmann's law assuming an emissivity equal to unity. PWV is the column precipitable water vapor, and LWP is the cloud liquid water path, both in centimeters. The regression coefficients  $a, b, c, d, e, f$  have values of 123.86, 0.444, 56.16,  $-3.65$ , 5.30, 1226.0, respectively. The algorithm was formulated based on detailed studies of radiative transfer models and observational data. The unique feature of this algorithm is that it uses one formula to compute the clear sky and all sky SDLW. The physical meaning of this algorithm can be explained as follows: the SDLW can be considered as contributions from the opaque regions of the longwave spectrum (for example,  $\text{H}_2\text{O}$  and  $\text{CO}_2$  bands) in which the downward LW radiation approximates to a blackbody, albeit the atmospheric emitting temperature rather than the surface skin temperature, while the PWV and LWP components dominate the window regions of the spectrum involving the water vapor continuum absorption and effective cloud base emission modified by sub-cloud absorption. These spectral regions are dynamic and depend upon the atmospheric profiles themselves. The LWP is used as a surrogate of effective cloud base height since LWP is found to be correlated with cloud base height based upon observational data and upon thermodynamic arguments by Hack [1998]. LWP is also better defined for any spatial and temporal grid. The algorithm was derived using observational data obtained

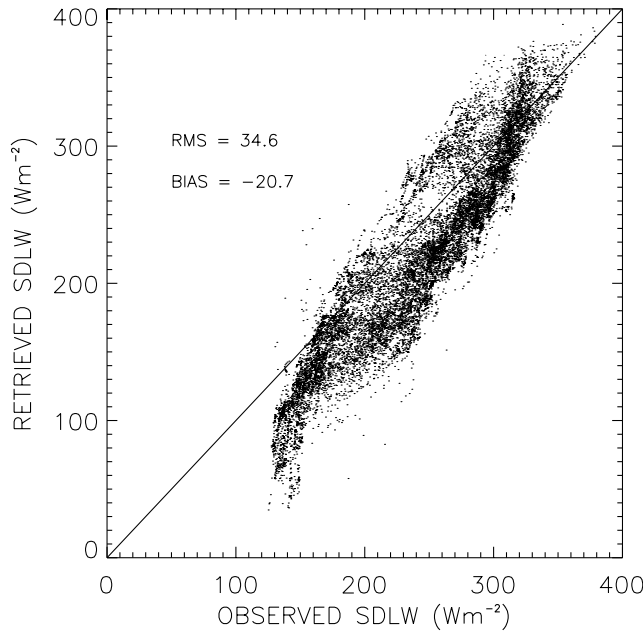


**Figure 1.** Scatterplot of observed SDLW versus SDLW calculated with original Zhou-Cess algorithm for ARM data from Barrow, NSA from January 2000 to December 2000.

from six Intensive Observation Periods (IOP) at the ARM SGP site and was verified with nine other SGP IOP data sets and TWP Manus data [Zhou and Cess, 2001]. The algorithm was not tested with observational data from other geophysical regions because of data availability problems.

## 2.2. The ARM NSA Data

[8] Recent climate modeling and diagnostic studies indicate the Polar Regions are particularly sensitive to global climate change and are important to mid-latitude climate and weather systems [Stammes *et al.*, 1999]. Radiation tends to dominate the Arctic heat budget in all seasons. Due to the extreme weather conditions experienced at high latitudes, the algorithms developed for mid-latitudes frequently do not work well for the Polar Regions. Thus, prudence necessitated testing the Zhou-Cess algorithm once high-quality observations from ARM NSA became available. The data used in the study were from January to December 2000 from the ARM Barrow facility, which is located at the northernmost point (71.32°N, 156.61°W) in the United States, 528 km north of the Arctic Circle. The data were taken from the same instruments and processed in the same manner as those used by Zhou and Cess [2001] for the SGP and TWP sites. The SDLW fluxes were pygeometer measurements, and the surface upwelling fluxes were computed from the Surface Meteorological Observation Station (SMOS) 2-m surface air temperature. The column precipitable water and cloud liquid water were both measured by microwave radiometers (MWR). All data were averaged into half-hour products. The results show that the algorithm mostly underestimates the SDLW, with large negative bias at the low SDLW (Figure 1). Further analysis found that 94% of the underestimated cases are related to very low water vapor amount (PWV < 0.81 cm). The low water vapor amount has resulted in very large negative value in the 3rd term in Eq. (1), i.e., the  $\ln(\text{PWV})$  term, since the logarithmic

function decreases very rapidly with decreasing water vapor below 1 cm. To remedy the problem, the  $\ln(\text{PWV})$  terms were replaced by  $\ln(1 + \text{PWV})$  to approximate a near-linear relationship between PWV and SDLW when water vapor amounts are very low. This modification has the added advantage of producing a very simple and reasonable relationship between the SDLW and the water vapor term which prevents the PWV from producing a negative contribution to the flux as the water vapor amounts asymptote toward zero.

[9] Although Zhou and Cess [2001] conducted radiative transfer calculations for six default Moderate-Resolution Transmittance Radiation Model [MODTRAN, Wang *et al.*, 1996] atmospheres (including subarctic summer and subarctic winter atmosphere) and their variations for providing basic relationships between SDLW and other parameters, the actual algorithm was derived using only observations at SGP site. For any nonlinear relationship, accounting for the full range of conditions is critical to derive statistical relationships that apply to most situations. This is because the statistical relations (usually derived with least squares fitting) will lean toward highly sampled situations and miss the under-sampled situations.

[10] The importance of sampling can be illustrated in Figure 2 where a linear relationship is calculated for

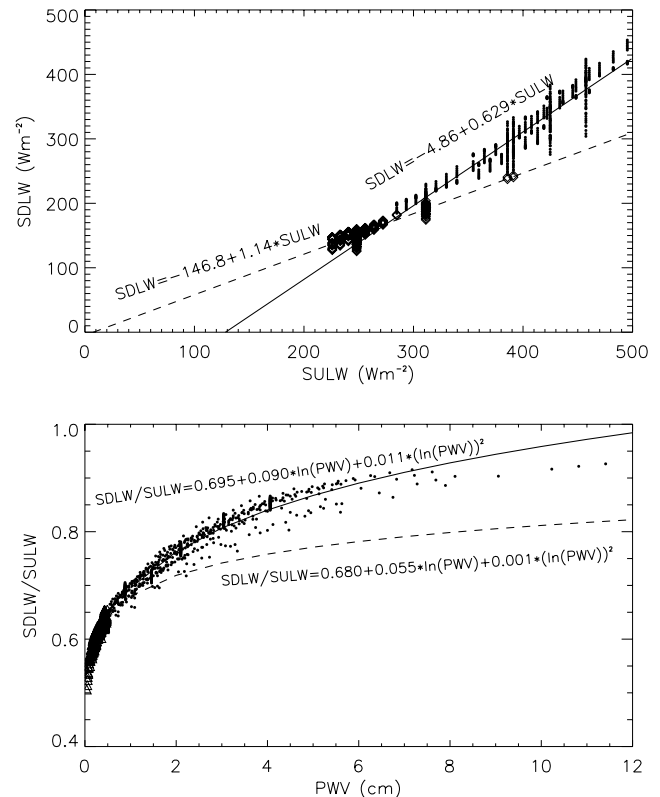


**Figure 2.** Relationships between MODTRAN computed clear sky SDLW and SULW (upper panel) and flux ratio versus column water vapor (lower panel). The black and dot lines are linear regression fits (upper panel) and log-square fits (lower panel) using data points with PWV greater than 0.5 cm (solid line) and PWV less than 0.5 cm (dash lines), respectively.



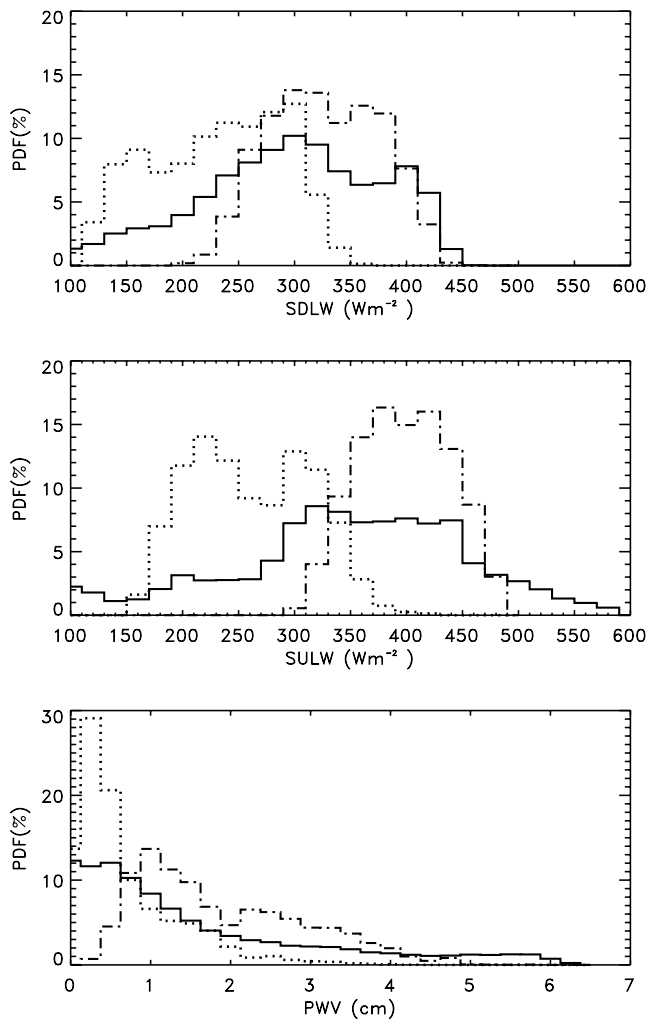


**Figure 3.** Normalized probability distribution functions of SDLW, SULW, and PWV from global network (solid line), ARM SGP site (dash-dot line), and ARM NSA site (dot line).

MODTRAN computed SDLW and SULW from Zhou and Cess [2001] (upper panel). Using the upper portion ( $PWV \geq 0.5$  cm) and the lower portion ( $PWV < 0.5$  cm) of the data gives very different slope and offset for a linear relationship. The log-square fit of PWV to the ratio of fluxes also depends significantly on different portions of the sampling data (lower panel). The reason why the SGP algorithm does not produce good results for NSA data is because SGP data only represents middle range of the data and thus is not applicable to the low end of the curve. Figure 3 illustrates the probability distribution functions (PDF) of SULW, SDLW, and PWV from global networks of 29 sites (Figure 4) and those from ARM SGP and NSA sites. An examination of Figure 3 reveals that the dynamical range of surface longwave fluxes and PWV from SGP misses a small fraction of data where SULW is larger than  $500 \text{ Wm}^{-2}$  or PWV greater than 5 cm as shown in the global PDFs. More importantly, however, the NSA PDFs clearly demonstrate that the distributions of these quantities largely misrepresent regions of extremely cold and dry areas. The misrepresentation of low water vapor situations

is particularly serious because of nonlinear logarithmic relationship between water vapor and SDLW.

[11] Due to data availability, the original algorithm only used cloud liquid water path to account for cloud effects to the SDLW. For the SGP and TWP site, the effect of ice clouds on the SDLW is relatively small since most of the ice clouds are at high altitudes. Such is not the case for the Polar Region, where most of the clouds are ice cloud located at low altitudes. Moreover, since the atmospheric water vapor concentrations for the Polar Regions are also very low, the effect of ice clouds on SDLW is not negligible.

### 3. Satellite Implementation

#### 3.1. Data

[12] The CERES single-scanner footprint (SSF) product contains 1 hour of instantaneous CERES data for a single-scanner instrument. The SSF product combines instantaneous CERES data with scene information and cloud properties derived from a high spatial resolution imager such as the Visible/Infrared Scanner (VIRS) on TRMM or the Moderate-Resolution Imaging Spectroradiometer (MODIS) on Terra and Aqua satellites. The cloud properties are computed in the cloud subsystem of CERES processing [Minnis *et al.*, 1997]. Thus, all of the input parameters for the Zhou-Cess algorithm are already computed or assembled in the current SSF processing.

[13] The ground measurements are taken from the CERES/ARM Validation Experiment [CAVE; Rutan *et al.*, 2001] database which is maintained at NASA LaRC in a Web-accessible form for use in the CERES project and is available to the outside science community. The surface observations used in this study include five ARM/SGP sites, one ARM/TWP site, seven National Surface Radiation Budget Network [SURFRAD; Augustine *et al.*, 2000] sites, eight Baseline Surface Radiation Network [BSRN; Ohmura *et al.*, 1998] sites, six Climate Monitoring and Diagnostics Laboratory (CMDL) sites, the LARC/COVE site [Jin *et al.*, 2002], and one NREL [Myers *et al.*, 1999] site (Figure 4). These sites were selected based on data availability and statistical representative of different geographical regions, i.e., ocean, land, desert, arctic regions. Temporal matching of the satellite and site fluxes was done at the highest resolution of the site data. Spatial matching was done to a distance of 10 km between the location of the site and the center of the CERES footprint. Values for all CERES footprints within the 10-km range of the sites and within the 1-minute interval were averaged together for comparison with the corresponding ground-based values.

[14] For the purposes of deriving, as well as validating a new algorithm, it is necessary to separate the training and validating data set. Here we have chosen 15 ground stations and collocated cloud parameters from Terra satellite during 58 months from March 2000 to December 2004 as a training data set. All 29 ground stations and their collocated Terra products for the same period are used in the validation since only clear and overcast portions of the training data set are used in the derivation of the algorithm. The collocated Aqua and ground measurements from all 29 stations covering the period from July 2002 to March 2005 serve as additional data set for validation.

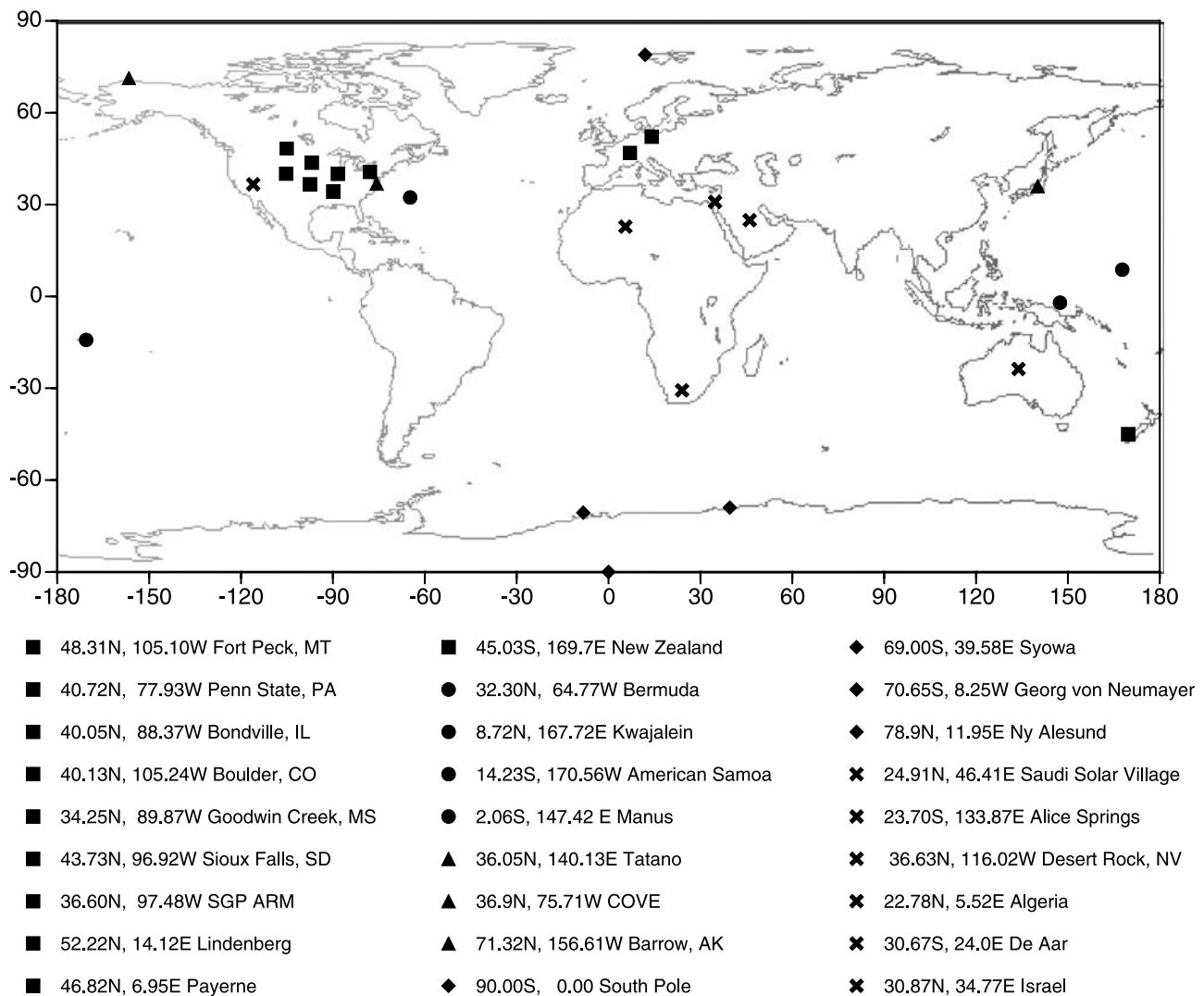


**Figure 4.** Ground stations used in this study.

### 3.2. Performance of the Original Algorithm

[15] Figure 5 shows the scatterplots of SDLW computed by the original Zhou-Cess algorithm for Terra satellite and collocated ground measurements from all 29 sites. For most geographical regions (continental, desert, island, and coastal area), the algorithm performs reasonably well; however, there is a significant underestimation of the SDLW in the Polar Regions, which is defined to include both the Arctic and Antarctic, when SDLW is below  $200 \text{ Wm}^{-2}$ . Most of the low values were observed at the South Pole where mean water vapor is only 0.38 mm. When the data are stratified with clear ( $f_{\text{clr}} > 0.999$ ), water cloud ( $\text{LWP} > 5 \text{ gm}^{-2}$ ), and ice cloud ( $\text{LWP} < 5 \text{ gm}^{-2}$  and ice water path ( $\text{IWP} > 1 \text{ gm}^{-2}$ ) cases, we find that there is positive bias for most of the clear sky cases except for some cases in Polar Regions. Large negative bias was found for both water cloud and ice cloud, with ice clouds having the largest negative bias (Figure 6). The large negative bias for cloudy sky flux might be due to lower cloud liquid water path generally observed from satellite than those observed from MWR at the SGP site. Our data indicates that the satellite rarely observes LWP greater than 1 mm over the SGP site while

MWR observes many cases with LWP greater than 1 mm (figure not shown). Other studies have also shown that LWP is rarely greater than 1.3 mm at SGP site [Huang *et al.*, 2003]. This leads us to suspect that some of the MWR measured cloud liquid water used in deriving the original algorithm might have been contaminated by rain or wetness from other forms of precipitation due to their unlikely larger value ( $\text{LWP} > 1.3 \text{ mm}$ ). The systematic difference between ice cloud and water cloud also indicates that ice clouds can play an important role for conditions other than the warm, moist tropical conditions. Taken together, these observations suggest that the algorithm should be re-derived using satellite observed cloud parameters and using more sites globally so that the algorithm better represents various atmospheric conditions. In the revised algorithm, the effect of ice cloud is considered by including ice water content in the same manner as cloud liquid water although with a smaller weight.

### 3.3. Revised Algorithm

[16] Based on the above analysis, a new algorithm is formulated which computes the fluxes for clear portions

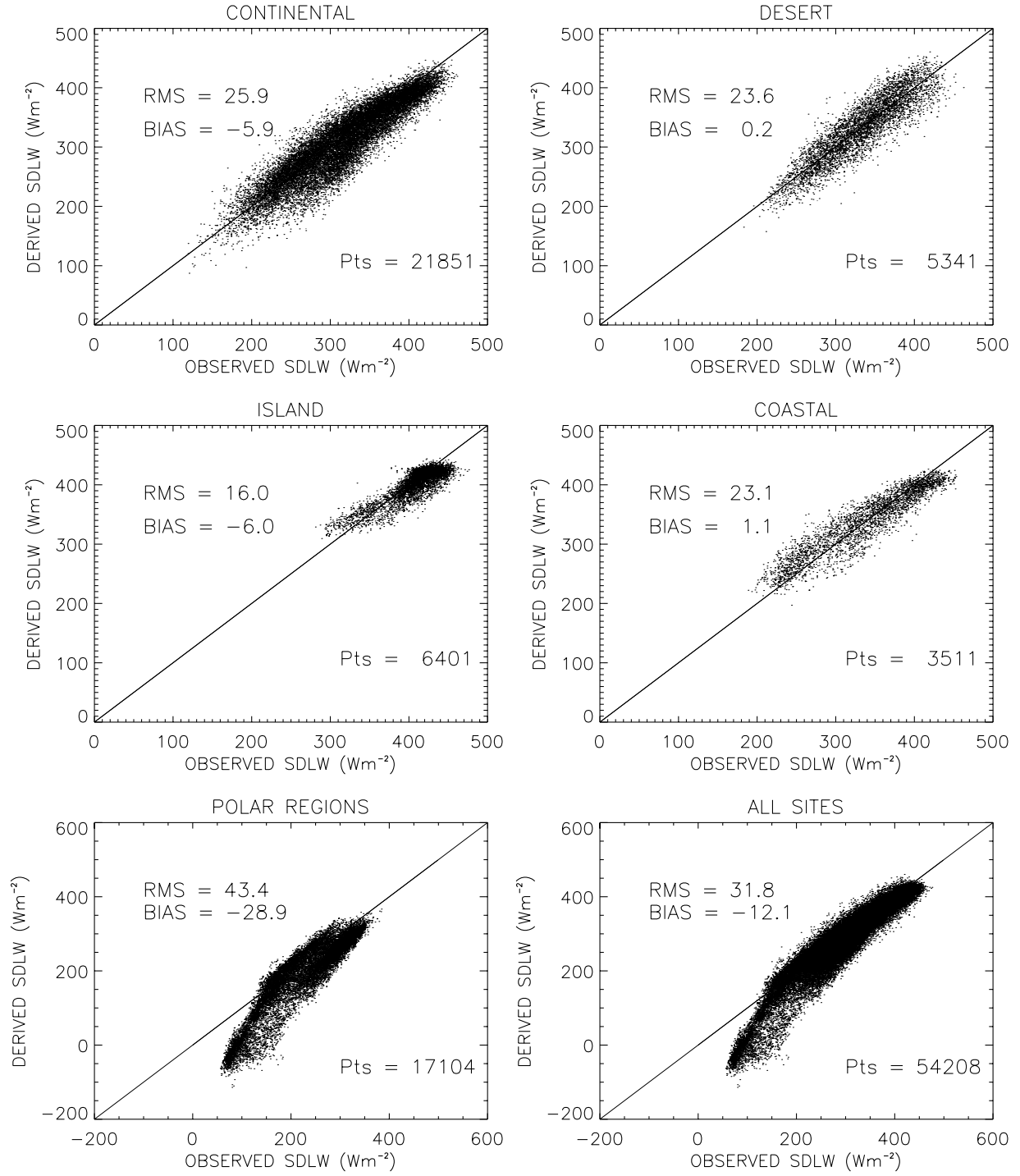


**Figure 5.** Scatterplots of SDLW computed using original Zhou-Cess algorithm for Terra satellite versus ground measurements for different scene types.

( $f_{\text{clr}}$ ) and cloudy portions ( $F_{\text{cld}}$ ) of the sky separately and then sums the results for the all sky flux ( $F_{\text{all}}$ ):

$$F_{\text{clr}} = a0 + a1 \cdot \text{SULW} + a2 \cdot \ln(1 + \text{PWV}) + a3 \cdot [\ln(1 + \text{PWV})]^2 \quad (2)$$

$$F_{\text{cld}} = b0 + b1 \cdot \text{SULW} + b2 \cdot \ln(1 + \text{PWV}) + b3 \cdot [\ln(1 + \text{PWV})]^2 + b4 \cdot \ln(1 + \text{LWP}) + b5 \cdot \ln(1 + \text{IWP})$$

(3)

$$F_{\text{all}} = F_{\text{clr}} \cdot f_{\text{clr}} + F_{\text{cld}} \cdot (1.0 - f_{\text{clr}}) \quad (4)$$

$$F_{\text{net}} = F_{\text{all}} - \text{SULW} \quad (5)$$

$$\begin{aligned} a0 &= 37.687, a1 = 0.474, a2 = 94.190, a3 = -4.935 \\ b0 &= 60.349, b1 = 0.480, b2 = 127.956, \\ b3 &= -29.794, b4 = 1.626, b5 = 0.535 \end{aligned}$$

where  $f_{\text{clr}}$  is the fraction of clear area in a single CERES footprint, and  $F_{\text{net}}$  is the net flux. SULW and PWV follow

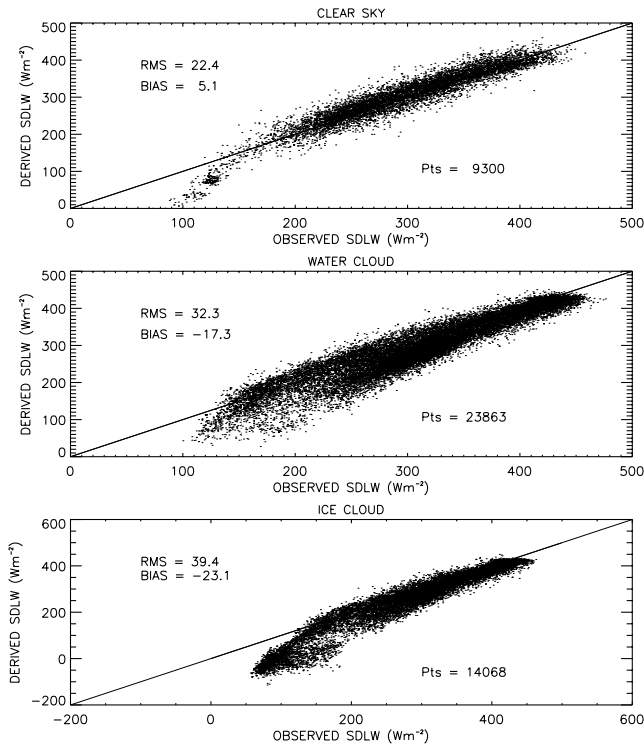


**Figure 6.** Scatterplots of SDLW computed using original Zhou-Cess algorithm versus ground measurements stratified for clear sky (Area<sub>clr</sub> > 99.9%), water cloud (LWP > 5 gm<sup>-2</sup>), and ice cloud (LWP < 5 gm<sup>-2</sup>, IWP > 1 gm<sup>-2</sup>) conditions for Terra satellite.

the same units as in (1). LWP and IWP (in gm<sup>-2</sup>) are not representative of the total for the pixel but only for the cloudy portion, since the cloud fraction is explicitly taken into consideration. The cloud fraction and cloud water path are part of SSF product and derived from CERES cloud analysis. The column precipitable water vapor is integrated from CERES meteorological data. Moreover, clear sky is defined when  $f_{clr}$  is greater than 0.999, and both LWP and IWP are set to zero. SULW is computed using a surface skin temperature with an emissivity of unity. Test cases run to incorporate a global emissivity map demonstrate no improvement in the algorithm. The physical bases of the algorithm are the same as the original algorithm, except that now clear sky and cloudy sky fluxes are computed separately. The presence of cloud changes the effective emitting layer of the atmosphere; hence the coefficients for SULW and PWV have changed accordingly. Notice that although the contribution of ice cloud has been given less weight, in the case of ice cloud on top of water cloud, the algorithm may produce bogus ice cloud contributions.

[17] As noted previously, the above regressions are derived using satellite observations from the Terra platform and matched ground measurements from 15 sites around the globe (Figure 4) from March 2000 to December 2004. There are 6028 clear sky cases ( $f_{clr} > 0.999$ ) for deriving the clear sky formula and 5788 overcast cases ( $f_{clr} < 0.01$ ) for the cloudy sky formula. These data consist of 43% of all collocated measurements in the training data set.

### 3.4. Validation

[18] The modified algorithm has been applied to the CERES Terra Edition 2B and Aqua Edition 2A SSF data products. The Terra Edition 2B data, as mentioned previously, spans the period from March 2000 to December 2004. The Aqua Edition 2A data cover the period from July 2002 to March 2005. Figure 7 illustrates the comparison of the SDLW of Terra Edition 2B computed with the modified Zhou-Cess algorithm versus the ground measured SDLW over 29 sites around the globe stratified for different scene types. The modified algorithm has smaller bias (less than 1 Wm<sup>-2</sup>) than the original algorithm for most of the scene types except for the coastal scenes where the systematic bias is 7.3 Wm<sup>-2</sup>. The scatterplots in Figure 8 of the derived versus measured SDLW show that the systematic bias from both water cloud and ice cloud is reduced and the difference between them is also reduced as compared to those from the original algorithm shown in Figure 6.

[19] The modified algorithm has also been applied to Aqua processing along with LWA and LWB, with the following results covering the 33 months from July 2002 to March 2005. The ground measurements are collected from the same 29 global sites as shown in Figure 4. All data available from these periods are used except for some data gaps. The validation was carried for clear sky and cloudy sky separately.

[20] Table 1 compares the bias and random error of the modified algorithm to those of the original algorithm as well as LWA and LWB for clear sky fluxes. Using the modified algorithm reduces the huge negative bias for the Polar Region from -137.0 Wm<sup>-2</sup> to an acceptable -10.5 Wm<sup>-2</sup>. The use of the modified algorithm has also resulted in improvement to either the bias or random error or both for most of the regions. The modified algorithm does produce biases for coastal and Polar Regions of the order of 10 Wm<sup>-2</sup>, whereas, globally, there is a less than 1 Wm<sup>-2</sup> bias and an 18 Wm<sup>-2</sup> random error. Comparison of the modified Zhou-Cess algorithm with LWA and LWB for clear sky fluxes shows that the modified algorithm has smaller bias for continental region than both LWA and LWB. The modified algorithm does however have larger systematic bias in the coastal and desert areas. The global mean bias is smaller probably due to cancellation of positive and negative biases. The random error of 18.5 Wm<sup>-2</sup> is slightly higher than those of LWA (17.7 Wm<sup>-2</sup>) and LWB (16.8 Wm<sup>-2</sup>).

[21] Table 2 compares the bias and random error of the modified Zhou-Cess algorithm to those of the original algorithm as well as LWB for cloudy sky fluxes (including partly cloudy cases). The results in Table 2 show that the major improvement for cloudy sky flux also occurs at Polar Region. The bias is reduced from -46.6 Wm<sup>-2</sup> to -0.89 Wm<sup>-2</sup>. There is also a modest improvement for the continental areas, though the bias is slightly larger for coastal and desert regions. Globally, the bias is 1.2 Wm<sup>-2</sup> with a random error of 23.6 Wm<sup>-2</sup>. Comparing cloud sky flux with those of LWB (note that LWA only computes clear sky flux), we find that the modified algorithm performs slightly better in continental, polar, desert, and island regions while only slightly worse in coastal areas.



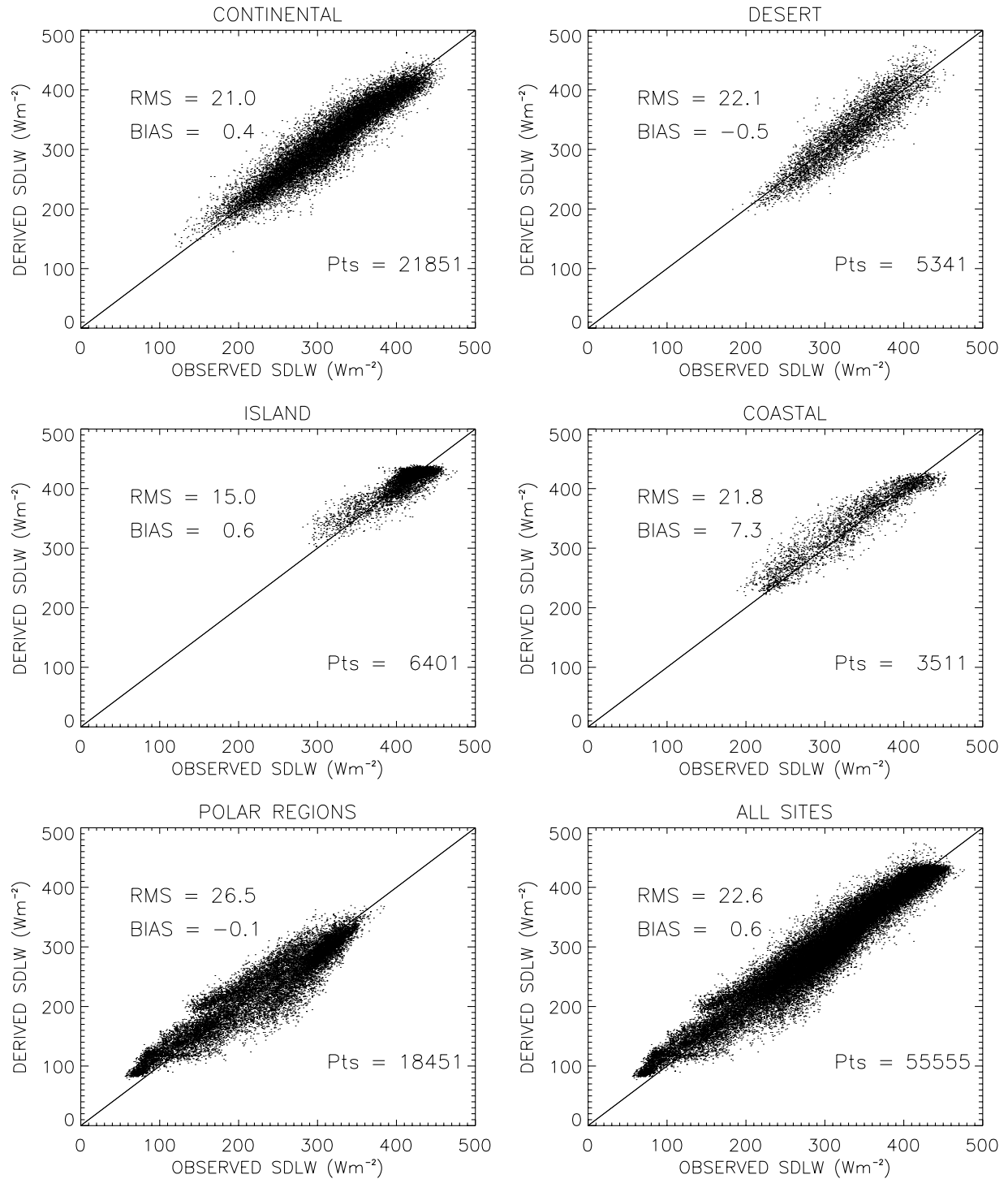


**Figure 7.** Scatterplots of SDLW computed using modified Zhou-Cess algorithm versus ground measurements for different scene types for Terra satellite from March 2000 to December 2004.

[22] Similar results for all sky fluxes (clear plus cloudy cases) are shown in Table 3. The modified algorithm shows improvements over original algorithm for most geographical regions in systematic error, except for coastal and island regions. Meanwhile, the random error is reduced for every region. The modified Zhou-Cess algorithm has slightly smaller systematic bias than LWB for all the regions except for the coastal region, which still has a

systematic bias of  $6.6 \text{ Wm}^{-2}$ . The global mean bias of all sky fluxes is  $1.1 \text{ Wm}^{-2}$ , and the random error is  $23.0 \text{ Wm}^{-2}$ , slightly better than LWB. Although the Zhou-Cess algorithm and LWB are very different algorithms, we have observed that the random errors of both models are fairly close to each other for each geographical region. This might be related with the spatial temporal collocation of satellite measurements with ground measure-

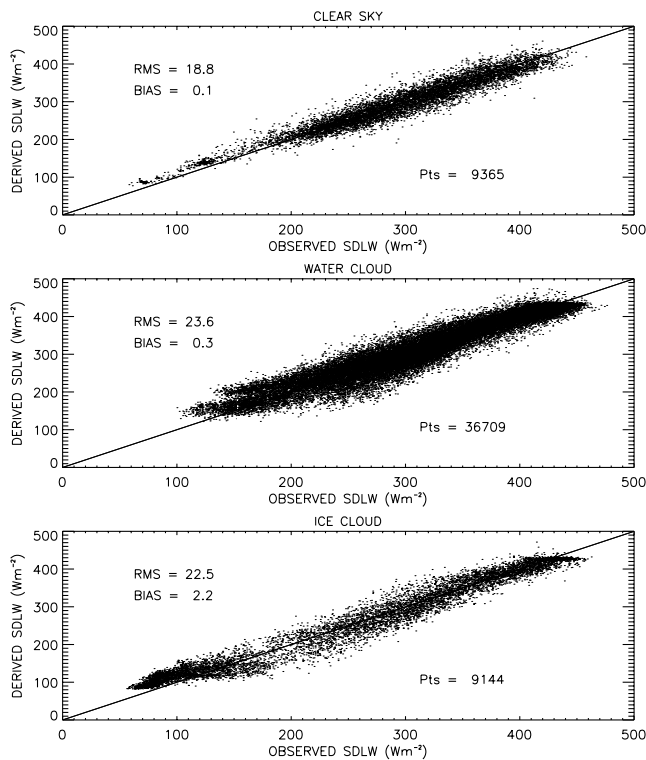


**Figure 8.** Scatterplots of SDLW computed using modified Zhou-Cess algorithm versus ground measurements stratified for clear sky (Area<sub>clr</sub> > 99.9%), water cloud (LWP > 5 gm<sup>-2</sup>), and ice cloud (LWP < 5 gm<sup>-2</sup>, IWP > 1 gm<sup>-2</sup>) conditions for Terra satellite from March 2000 to December 2004.

ments and the uncertainties associated with satellite retrieved cloud parameters, i.e., cloud fraction used in both algorithms. According to Dong et al. (X. Dong et al., Comparison of CERES-MODIS stratus cloud properties with ground-based measurements at the DOE ARM Southern Great Plains site, submitted to *Journal of Geophysical Research*, 2007), there is about 30–50% of uncertainty of CERES-derived LWP in comparison with ground radar and lidar-based observations at ARM SGP site. The IWP retrieval could also be biased for 30% by neglecting multilayer cloud in the current one-layer cloud retrieval

algorithm for multilayer clouds [Huang et al., 2005]. The above estimates of errors/biases in the CERES cloud property retrievals are based on ARM SGP data. There is limited knowledge over other geographical regions. The errors and uncertainties in these cloud parameters can contribute to large standard deviations in the derived fluxes.

[23] Despite the overall good performance, there are still a few noticeable drawbacks with the current algorithm. First of all, this algorithm is empirically derived, and the exact regression coefficients are subject to the specific training data set. Uneven sampling and errors in the training data set will be carried into the algorithm. We noticed that the algorithm seems to overestimate at very low SDLW (<100 Wm<sup>-2</sup>) and underestimate at very high SDLW (>420 Wm<sup>-2</sup>) (Figure 7). This may partly be due to small number of samples and measurement errors associated with extreme cases in the training data set. The slight positive bias for low SDLW is dominated by comparison in the Polar Region which is notorious for challenging even the best cloud retrieval algorithms. The other reason may be due to a fixed linear relationship between SDLW and SULW. From the lower panel of Figure 2, we have seen that the ratio of SDLW/SULW increases with increasing column water vapor so that the fixed slope of SULW in our algorithm is partly compensated by the PWV term. However, the algorithm's treatment of SULW and PWV as independent terms might have limited coupling between SULW and PWV at extreme conditions and hence limited its dynamic range.

[24] There are also a few regions or stations that present quite large biases. It is found that the large bias of coastal area mainly comes from the COVE (Chesapeake light house, 36.90°N, 75.71°W) site which has a positive bias of 18.6 Wm<sup>-2</sup>. A few other sites, namely, Fort Peck (FPK, 48.31°N, 105.10°W), Sioux Falls (SXF, 43.73°N, 96.92°W), Payerne (PAY, 46.82°N, 6.95°E), and the South Pole (SPL) also have systematic bias larger than 10 Wm<sup>-2</sup>. The causes for the large biases in these sites may be related with specific conditions of the sites and should be examined individually.

[25] Gupta et al. [2004] found that systematic bias of LWB varies with instrument network and day-night skin temperature bias. To rule out that some of the systematic bias might be due to instrument setup, we computed the

**Table 1.** Error Statistics of Longwave Clear Sky Fluxes Computed From Zhou-Cess Algorithm (Original and Modified), LWA and LWB Against Surface Measurements for Aqua Satellite From July 2002–March 2005

Sites		Original	Modified		
# of Points		Zhou-Cess	Zhou-Cess	LWA	LWB
Continental	Bias Wm <sup>-2</sup> (%)	6.71 (2.38)	-0.16 (-0.06)	-4.48 (-1.59)	-6.93 (-2.46)
5012	$\sigma$ Wm <sup>-2</sup> (%)	20.9 (7.4)	16.6 (5.9)	15.8 (5.6)	15.4 (5.5)
Coastal	Bias Wm <sup>-2</sup> (%)	16.66 (5.84)	10.03 (3.52)	4.92 (1.72)	-0.15 (-0.05)
609	$\sigma$ Wm <sup>-2</sup> (%)	17.8 (6.3)	14.8 (5.2)	12.9 (4.5)	13.2 (4.6)
Polar Regions	Bias Wm <sup>-2</sup> (%)	-137.0 (122.0)	10.45 (9.30)	-16.0 (14.30)	-8.83 (-7.88)
903	$\sigma$ Wm <sup>-2</sup> (%)	34.5 (30.7)	11.1 (9.9)	11.0 (9.9)	11.0 (9.9)
Desert	Bias Wm <sup>-2</sup> (%)	-1.68 (-0.53)	-7.12 (-2.27)	-0.41 (-0.13)	-5.15 (-1.64)
1640	$\sigma$ Wm <sup>-2</sup> (%)	24.4 (7.8)	23.9 (7.6)	22.8 (7.3)	21.1 (6.7)
Island	Bias Wm <sup>-2</sup> (%)	9.31 (2.47)	2.92 (0.77)	-0.75 (-0.20)	-0.77 (-0.20)
138	$\sigma$ Wm <sup>-2</sup> (%)	10.3 (2.7)	12.6 (3.3)	12.0 (3.2)	13.8 (3.6)
Global	Bias Wm <sup>-2</sup> (%)	-9.81 (-3.61)	0.42 (0.15)	-4.18 (-1.54)	-6.19 (-2.28)
8302	$\sigma$ Wm <sup>-2</sup> (%)	41.4 (15.3)	18.5 (6.8)	17.7 (6.5)	16.8 (6.2)

**Table 2.** Error Statistics of Longwave Cloudy Sky Fluxes Computed Using Zhou-Cess Algorithm (Original, Modified) and LWB Against Surface Measurements for Aqua Satellite From July 2002–March 2005

Sites		Original	Modified	LWB
# of Points		Zhou-Cess	Zhou-Cess	
Continental	Bias $\text{Wm}^{-2}$ (%)	−7.42 (−2.33)	0.61 (0.19)	−3.38 (−1.06)
21117	$\sigma \text{ Wm}^{-2}$ (%)	28.0 (8.8)	22.6 (7.1)	22.4 (7.0)
Coastal	Bias $\text{Wm}^{-2}$ (%)	1.80 (0.52)	6.00 (1.72)	2.51 (0.72)
3302	$\sigma \text{ Wm}^{-2}$ (%)	21.2 (6.1)	18.5 (5.3)	19.0 (5.4)
Polar Regions	Bias $\text{Wm}^{-2}$ (%)	−46.63 (−20.17)	−0.89 (−0.39)	−6.17 (−2.67)
17663	$\sigma \text{ Wm}^{-2}$ (%)	50.6 (21.9)	23.6 (10.2)	25.0 (10.8)
Desert	Bias $\text{Wm}^{-2}$ (%)	8.19 (2.42)	9.67 (2.85)	11.88 (3.51)
4170	$\sigma \text{ Wm}^{-2}$ (%)	28.1 (8.3)	27.7 (8.2)	28.8 (8.5)
Island	Bias $\text{Wm}^{-2}$ (%)	0.58 (0.14)	0.95 (0.23)	5.71 (1.39)
6729	$\sigma \text{ Wm}^{-2}$ (%)	13.5 (3.3)	12.5 (3.0)	14.8 (3.6)
Global	Bias $\text{Wm}^{-2}$ (%)	−17.67 (−5.80)	1.20 (0.39)	−1.59 (−0.52)
52981	$\sigma \text{ Wm}^{-2}$ (%)	40.1 (13.2)	23.6 (7.8)	24.4 (8.0)

biases grouped with different network. Table 4 shows no discernible trends in systematic biases between different networks. The ARM instruments have smaller random error because four out of five instruments are clustered in the ARM SGP site. The BSRN instruments have the largest random error due to varied geographical locations of the measurements. The small systematic bias should not be contributed to instruments themselves.

[26] The systematic differences between daytime and nighttime biases, however, are found for all sky fluxes from both Terra and Aqua platforms (Table 5). The revised algorithm 4 overestimates the daytime SDLW by 3–4  $\text{Wm}^{-2}$  and underestimates nighttime SDLW by 2–3  $\text{Wm}^{-2}$ . This might be related to the use of skin temperature estimates. The original algorithm uses 2-m air temperature which is more closely related to the lower atmosphere and hence the SDLW. Another problem of  $T_{\text{skin}}$  or 2-m temperature arises in regions of anomalous temperature lapse rate. For example, desert regions can have super-adiabatic lapse rates so 2-m temperature overestimates the effective emission level temperature. Conversely, temperature inversions are common for high latitude regions so 2-m temperature may underestimate the effective emitting temperature. An investigation is currently underway at NASA Langley Research Center to use a constrained surface temperature in the CERES surface radiation product since all of the LW models tend to

overestimate the surface downward LW radiation for cases where the surface temperatures are significantly higher than the air temperatures. The modified skin temperature (or constrained temperature) might help reduce the day-night bias and also the overall bias in this algorithm and others.

### 3.5. Tibet Site

[27] Besides the Polar Region, the Tibet plateau represents another kind of special conditions (low temperature, low humidity, and low atmosphere mass) due to its high elevation. This special condition leads to high shortwave radiation and low longwave radiation. Yang *et al.* [2006] have found that current satellite products have much larger negative biases in LW in Tibet (40  $\text{Wm}^{-2}$ ) than in other regions. It is natural to examine whether the new algorithm will work in such special conditions. More importantly, Tibet is a key region for Asian monsoon, and the summer heating over the plateau is strongly related to the onset and withdraw of the Asian monsoon. A validated radiation product for studies of Tibet heating is much desired by Tibet research community.

[28] Since coincident surface radiation measurements and CERES SSF data are very rare, which makes direct validation impossible at this time, we have used an indirect method to demonstrate that our revised algorithm works well in high altitude regions, such as Tibet. First, we show

**Table 3.** Error Statistics of Longwave All Sky Fluxes Computed Using Zhou-Cess Algorithm (Original, Modified) and LWB Against Surface Measurements for Aqua Satellite From July 2002–March 2005

Sites		Original	Modified	LWB
# of Points		Zhou-Cess	Zhou-Cess	
Continental	Bias $\text{Wm}^{-2}$ (%)	−4.71 (−1.51)	0.46 (0.15)	−4.06 (−1.31)
26129	$\sigma \text{ Wm}^{-2}$ (%)	27.2 (8.7)	21.6 (6.9)	21.3 (6.8)
Coastal	Bias $\text{Wm}^{-2}$ (%)	4.12 (1.21)	6.63 (1.95)	2.10 (0.62)
3911	$\sigma \text{ Wm}^{-2}$ (%)	20.9 (6.1)	18.1 (5.3)	18.4 (5.4)
Polar Regions	Bias $\text{Wm}^{-2}$ (%)	−51.03 (−22.64)	−0.34 (−0.15)	−6.30 (−2.79)
18566	$\sigma \text{ Wm}^{-2}$ (%)	51.6 (22.9)	23.3 (10.3)	24.8 (11.0)
Desert	Bias $\text{Wm}^{-2}$ (%)	5.40 (1.63)	4.93 (1.48)	7.08 (2.13)
5810	$\sigma \text{ Wm}^{-2}$ (%)	27.5 (8.3)	27.4 (8.3)	27.3 (8.2)
Island	Bias $\text{Wm}^{-2}$ (%)	0.76 (0.19)	0.99 (0.24)	5.58 (1.36)
6867	$\sigma \text{ Wm}^{-2}$ (%)	13.5 (3.3)	12.5 (3.1)	14.8 (3.6)
Global	Bias $\text{Wm}^{-2}$ (%)	−16.61 (−5.54)	1.09 (0.36)	−2.22 (−0.74)
61283	$\sigma \text{ Wm}^{-2}$ (%)	41.1 (13.7)	23.0 (7.7)	23.5 (7.8)

**Table 4.** Biases of Longwave All Sky Fluxes Computed Using Zhou-Cess Algorithm Compared With Surface Measurements Stratified With Observational Network

Platform		ARM	SURF	BSRN	CMDL
Terra	Bias $\text{Wm}^{-2}$	1.1	2.9	-3.1	0.5
	$\sigma$ $\text{Wm}^{-2}$	17.6	22.2	26.2	21.2
Aqua	Bias $\text{Wm}^{-2}$	2.7	0.9	-0.2	-1.1
	$\sigma$ $\text{Wm}^{-2}$	18.8	22.6	27.6	21.1

that our revised algorithm produces a significant improvement over dry, cold conditions while making little changes under other conditions. This is done by comparing the original Zhou-Cess algorithm with LWB and the revised Zhou-Cess algorithm with LWB for January 2005 and July 2005, respectively, over a validation subset on Tibet plateau ( $89^{\circ}\text{E}$ – $90^{\circ}\text{E}$ ,  $33^{\circ}\text{N}$ – $34^{\circ}\text{N}$ ). Here we used LWB, which is also used in the GEWEX SRB effort, as a surrogate for surface measurements. The upper panel of Figure 9 shows a comparison between the old model and LWB in cross symbol, and a comparison between the revised model and LWB in square symbol. As we can see, for cold, dry January conditions, the comparison between the revised model and LWB is much improved over the comparison between the old model and LWB. In contrast, the lower panel of Figure 9 shows results for warmer, somewhat wetter July conditions, where little difference is seen among the old model, the new model, and LWB regardless of the altitude.

[29] Next, we show that the LWB results compare quite well with the surface measurements at the Tibet site and thus represent surface measurements in Figure 9. Since the only surface data available for the Tibet site, which were also coincident with CERES measurements, were for the warmer, somewhat wetter months from late May through September 1998 during GEWEX Asian Monsoon Experiment–Tibet [GAME–Tibet, Koike *et al.*, 1999], we have instead shown a comparison between LWB derived fluxes and that surface measurements from Naqu, Tibet ( $91.54^{\circ}\text{E}$ ,  $31.38^{\circ}\text{N}$ ) (Figure 10). At first glance, the comparison appears to have more RMS than what is considered ideal; however, it is noted that the scatter of points in the upper part of the plot is due to relatively high skin temperatures in relation to near surface air temperatures. This is a known problem, which often occurs over areas such as desert in the summer and the Sea of Japan in winter, and which will be addressed in CERES Edition 3. The slightly negative bias is an artifact of the surface being at an altitude which is significantly lower than the grid box altitude [Yang *et al.*, 2006]. This

**Table 5.** Biases of Longwave All Sky Fluxes Computed Using Zhou-Cess Algorithm Compared With Surface Measurements Stratified With Observational Time

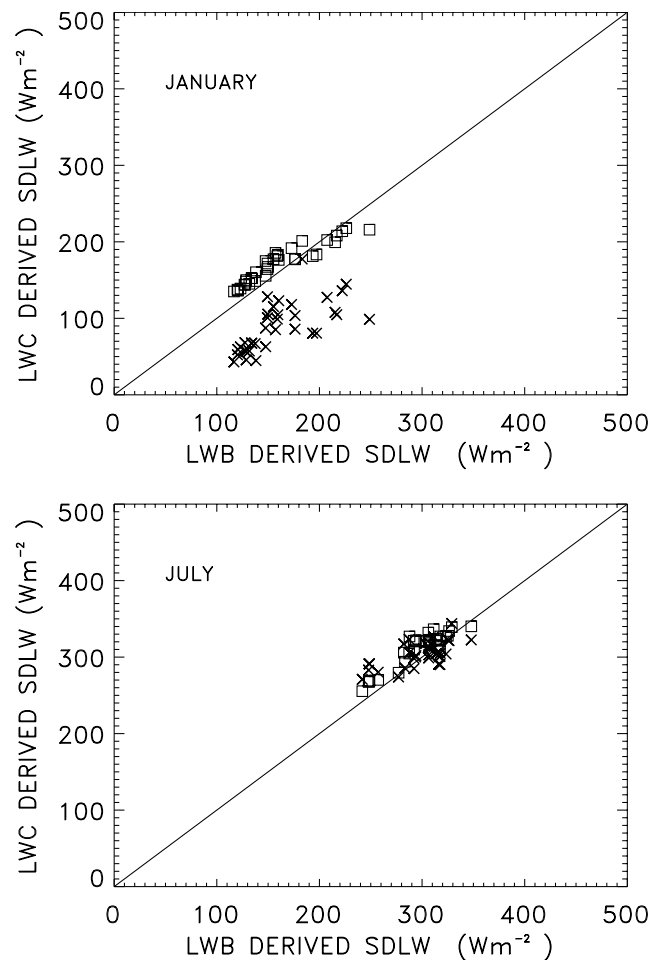
Platform		Daytime	Nighttime
Terra	Bias $\text{Wm}^{-2}$	4.9	-3.4
	$\sigma$ $\text{Wm}^{-2}$	15.7	24.3
Aqua	Bias $\text{Wm}^{-2}$	3.5	-2.3
	$\sigma$ $\text{Wm}^{-2}$	20.9	24.2

means that LWB is calculating a surface flux which is over 300 m higher than the surface site, which should cause the negative bias. The conclusion is that LWB represents surface measurements reasonably well over the Tibet site.

[30] Together, these results suggest that the revised Zhou-Cess algorithm is an improvement over the old model for cold, dry conditions while making little changes under other conditions, and there seems to have no systematic bias associated with high elevations as demonstrated with Tibet data. Of course, the performance of the algorithm will rely highly on the accuracy of input parameters such as surface temperature and column water vapor as with other long-wave algorithms.

#### 4. Conclusions and Discussions

[31] An improved version of Zhou-Cess algorithm has been formulated which avoids the large errors in the SDLW at low water vapor conditions by adding an offset to the logarithmic water vapor term. The new algorithm also

**Figure 9.** Comparisons of SDLW computed by original (cross) and modified (square) Zhou-Cess algorithms versus LWB for January (upper panel) and July (lower panel) 2005, respectively, over a Tibet validation site located at ( $33$ – $34^{\circ}\text{N}$ ,  $89$ – $90^{\circ}\text{E}$ ).



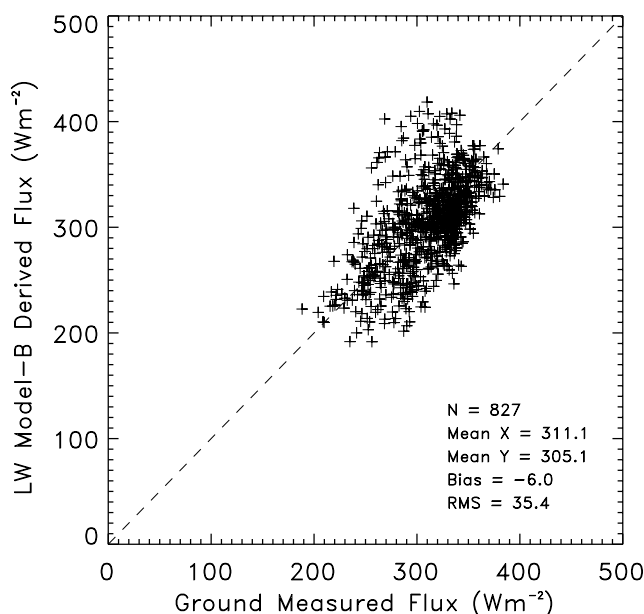


**Figure 10.** Comparison of ground measured surface downwelling longwave fluxes and LWB derived fluxes over Naqu, Tibet site during May to September 1998.

utilizes cloud fraction and cloud liquid and ice water paths available from the CERES SSF product to separately compute the clear and cloudy portions of the flux. The new algorithm has been validated for the Terra and Aqua satellites against surface measurements at 29 stations around the globe. The results show significant improvement over the original version and are comparable or slightly better than the more complicated algorithms currently implemented in the CERES processing. Preliminary tests also suggest that the new algorithm works quite as well for high elevation locations such as Tibet site. This revised version of the Zhou-Cess algorithm will be incorporated into the CERES operational processing.

[32] The SDLW fluxes generated for the CERES SSF should be an instantaneous product with input from instantaneous satellite retrieved cloud parameters and PWV derived from meteorological products. The accuracy of the algorithm will depend on these input parameters. It is mostly applicable to producing maps of the surface radiation budget rather than for determining accurate variability or trends over time. The latter would require very stable, well-calibrated input of PWV, LWP, IWP. The current algorithm assumes a fixed linear relationship between SDLW and SULW, which seems to allow smaller dynamic range of SDLW than those of observed SDLW. A better training data set with high quality input data and more coverage of extreme dynamic range may help improve the algorithm if such data set is available.

[33] **Acknowledgments.** The first author is supported by NASA Interdisciplinary Research in Earth Science NRA-02-OES-06 under WBS 509496.02.01.01.07, UPN 291-01-97-05 and UPN 291-01-c7 and is much grateful to Arthur. Y. Hou for his support and Warren Wiscombe for his insightful comments on the manuscript. The authors thank anonymous reviewers of the paper for their constructive comments that helped improve the manuscript. The CERES SRB project is sponsored by

WBS 921266.04.07.07. ARM data are made available through the U.S. Department of Energy as part of the Atmospheric Radiation Measurement Program.

## References

- Augustine, J. A., J. J. DeLuisi, and C. N. Long (2000), SURFRAD-A National Surface Radiation Budget Network for Atmospheric Research, *Bull. Am. Meteorol. Soc.*, **81**, 2341–2358.
- Charlock, T. P., et al. (1997), Compute surface and atmospheric fluxes (system 5.0): CERES Algorithm Theoretical Basis Document (Release 2.2), NASA/RP-1376, 84 p. [Available online at [asd www.larc.nasa.gov/ATBD/ATBD.html](http://asd-www.larc.nasa.gov/ATBD/ATBD.html)]
- Cox, S. J., et al. (2006), The NASA/GEWEX Surface Radiation Budget Project: Overview and analysis, paper presented at 12th Conference on Atmospheric Radiation, *AM. Meteorol. Soc. Madison, Wis.*
- Darnell, W. L., W. F. Staylor, S. K. Gupta, N. A. Ritchey, and A. C. Wilber (1992), Seasonal variation of surface radiation budget derived from ISCCP-C1 data, *J. Geophys. Res.*, **97**, 15,741–15,760.
- Gupta, S. K., W. L. Darnell, and A. C. Wilber (1992), A parameterization for longwave surface radiation from satellite data: Recent improvements, *J. Appl. Meteorol.*, **31**, 1361–1367.
- Gupta, S. K., D. P. Kratz, A. C. Wilber, and L. C. Nguyen (2004), Validation of parameterized algorithms used to derive TRMM-CERES surface radiative flux, *J. Atmos. Oceanic. Technol.*, **21**, 742–752.
- Hack, J. J. (1998), Sensitivity of the simulated climate to a diagnostic formulation for cloud liquid water, *J. Clim.*, **11**, 1497–1515.
- Huang, J. P., P. Minnis, B. Lin, M. M. Khaiyer, P. W. Heck, and T.-F. Fan (2003), Determination of ice-water path over the ARM SGP using combined surface and satellite datasets. Proceedings of the Thirteenth Atmospheric Radiation Measurement (ARM) Science Team Meeting ARM-CONF-2003, April 2003 Broomfield, Colorado.
- Huang, J., P. Minnis, B. Lin, Y. Yi, M. M. Khaiyer, R. F. Arduini, and G. G. Mace (2005), Advanced retrievals of multilayered cloud properties using multi-sensor and multi-spectral measurements, *J. Geophys. Res.*, **110**, D15518, doi:10.1029/2004JD005101.
- Inamdar, A. K., and V. Ramanathan (1997), On monitoring the atmospheric greenhouse effect from space, *Tellus*, **49B**, 216–230.
- Jin, Z., T. P. Charlock, and K. Rutledge (2002), Analysis of the broadband solar radiation and albedo over the ocean surface at COVE, *J. Atmos. Oceanic. Technol.*, **19**, 1585–1601.
- Koike, T., T. Yasunari, J. Wang, and T. Yao (1999), GAME-Tibet IOP summary report, paper presented at 1st International Workshop on GAME-Tibet, *Jpn. Soc. Snow Ice, Xi'an, China*.
- Li, Z., H. G. Leighton, and R. D. Cess (1993), Surface net solar radiation estimated from satellite measurements: Comparisons with tower observations, *J. Clim.*, **6**, 1764–1772.
- Minnis, P., et al. (1997), Cloud optical property retrieval (system 4.3). CERES Algorithm Theoretical Basis Document (Release 2.2), NASA/RP-1376, 60 p. [Available online at [asd www.larc.nasa.gov/ATBD/ATBD.html](http://asd-www.larc.nasa.gov/ATBD/ATBD.html)]
- Myers, D. R., S. Wilcox, M. Anderberg, S. H. Alawaji, N. M. Al Abbadi, and M. Y. bin Mahfoudh (1999), Saudi Arabian solar radiation network of data for validating satellite remote-sensing systems, *Earth Obs. Sys. IV SPIE Vol 3750*, 18–20 July, Denver CO.
- Ohmura, A., et al. (1998), Baseline Surface Radiation Network (BSRN/WCRP): New precision radiometry for climate change research, *Bull. Am. Meteorol. Soc.*, **79**, 2115–2136.
- Ramanathan, V. (1986), Scientific use of surface radiation budget data for climate studies, surface radiation budget for climate application edited by J. T. Suttles and G. Ohring, Publ. 1169, NASA, Washington, DC.
- Rutan, D. A., F. G. Rose, N. M. Smith, and T. P. Charlock (2001), Validation data set for CERES surface and atmospheric radiation budget (SARB), WCRP/GEWEX Newsletter, **11**(1), 11–12. [Available online at [www.gewex.org/feb01.pdf](http://www.gewex.org/feb01.pdf); data available online at [www-cave.larc.nasa.gov/cave/](http://www-cave.larc.nasa.gov/cave/)]
- Stamnes, K., R. G. Ellingson, J. A. Curry, J. E. Walsh, and B. D. Zak (1999), Review of science issues, deployment strategy, and status for the ARM north slope of Alaska—Adjacent Arctic Ocean Climate Research Site, *J. Clim.*, **12**, 46–63.
- Stephens, G. L., and P. J. Webster (1984), Cloud decoupling of the surface and planetary radiative budgets, *J. Atmos. Sci.*, **41**, 681–686.
- Stokes, G. M., and S. E. Schwartz (1994), The Atmospheric Radiation Measurement (ARM) program: Programmatic background and design of the cloud and radiation testbed, *Bull. Am. Meteorol. Soc.*, **75**, 1201–1221.
- Wang, J., G. P. Anderson, H. E. Revercomb, and R. O. Knutson (1996), Validation of FASCOD3 and MODTRAN3: Comparison of model calculations with ground-based and airborne interferometer observations under clear-sky conditions, *Appl. Opt.*, **35**, 6028–6040.

- Wielicki, B. A., B. R. Barkstrom, E. F. Harrison, R. B. Lee III, G. L. Smith, and J. E. Cooper (1996), Clouds and the Earth's Radiant Energy System (CERES): An Earth Observing System experiment, *Bull. Am. Meteorol. Soc.*, **77**, 853–868.
- Yang, K., T. Koshio, P. Stackhouse, C. Mikovitz, and J. Cox (2006), An assessment of satellite radiation products for highlands with Tibet instrumental data, *Geophys. Res. Lett.*, **33**, L22403, doi:10.1029/2006GL027640.
- Zhang, Y.-C., W. B. Rossow, A. A. Lacis, V. Oinas, and M. L. Mishchenko (2004), Calculation of radiative fluxes from the surface to top of atmosphere based on ISCCP and other global data sets: Refinements of the radiative transfer model and the input data, *J. Geophys. Res.*, **109**, D19105, doi:10.1029/2003JD004457.
- Zhou, Y. P., and R. D. Cess (2001), Algorithm development strategies for retrieving the downwelling longwave flux at the Earth's surface, *J. Geophys. Res.*, **106**, 12,477–12,488.
- 
- R. D. Cess, Marine Sciences Research Center, S.U.N.Y. at Stony Brook, Stony Brook, New York, USA.
- D. P. Kratz, Climate Science Branch, NASA Langley Research Center, Hampton, Virginia, USA.
- S. K. Gupta and A. C. Wilber, Analytical Services & Materials, Inc., Hampton, Virginia, USA.
- Y. Zhou, Goddard Earth Sciences & Technology Center, University of Maryland Baltimore County, Catonsville, Maryland, USA. (yaping.zhou.1@gssc.nasa.gov; yapingzhou@hotmail.com)